

THE MAGNETAR 1E 1547.0–5408: RADIO SPECTRUM, POLARIMETRY, AND TIMING

F. CAMILO,¹ J. REYNOLDS,² S. JOHNSTON,³ J. P. HALPERN,¹ AND S. M. RANSOM⁴*Received 2007 December 17; accepted 2008 January 31*

ABSTRACT

We have investigated the radio emission from the anomalous X-ray pulsar 1E 1547.0–5408 (PSR J1550–5418) using the Parkes telescope and the Australia Telescope Compact Array. The flux density of the pulsar is roughly the same between 1.4 and 45 GHz, but shows time variability. The radiation is nearly 100% linearly polarized between frequencies of 45 and 3.2 GHz, but from 2.3 to 1.4 GHz it becomes increasingly more depolarized. The rotation measure of -1860 rad m^{-2} is the largest for any known pulsar, and implies an average magnetic field strength along the line of sight of $2.7 \mu\text{G}$. The pulse profiles are circularly polarized at all frequencies observed, more so at lower frequencies, at the $\approx 15\%$ level. The observed swing of the position angle of linear polarization as a function of pulse phase suggests that in this neutron star the rotation and magnetic axes are nearly aligned, and that its radio emission is only detectable within a small solid angle. Timing measurements indicate that the period derivative of this 2 s pulsar has increased by nearly 40% in a 6-month period. The flat spectrum and variability in flux density and pulse profiles are reminiscent of the properties of XTE J1810–197, the only other known radio-emitting magnetar, and are anomalous by comparison with those of ordinary radio pulsars.

Subject headings: ISM: individual (G327.24–0.13) — pulsars: individual (1E 1547.0–5408, PSR J1550–5418, XTE J1810–197) — stars: neutron

1. INTRODUCTION

Anomalous X-ray pulsars (AXPs) and soft gamma-ray repeaters are neutron stars whose long rotation periods (2–12 s) are a result of very strong surface magnetic fields (see Woods & Thompson 2006 for a review). In the magnetar model (Duncan & Thompson 1992; Thompson & Duncan 1995, 1996), their large and variable X-ray luminosity is a result of magnetic field decay, but much remains unknown about this class of young neutron stars.

Two of the 13 confirmed magnetars are radio emitters. The 5 s AXP XTE J1810–197 shows remarkable pulsations (Camilo et al. 2006) that have a flat spectrum (Camilo et al. 2007c) and are highly linearly polarized (Camilo et al. 2007d; Kramer et al. 2007). Its flux density and pulse profile vary greatly on short timescales (Camilo et al. 2007a). This radio emission (Halpern et al. 2005) arose only after an X-ray outburst (Ibrahim et al. 2004).

The AXP 1E 1547.0–5408, recently identified at the center of the candidate supernova remnant G327.24–0.13 (Gelfand & Gaensler 2007), emits radio waves at the rotation period $P = 2$ s (Camilo et al. 2007b). These are transient, and are apparently related to the X-ray variability shown by the AXP (Halpern et al. 2008). Here we report on a detailed study of the radio emission from 1E 1547.0–5408 (PSR J1550–5418), and compare its spectral, polarimetric, and timing properties to those of XTE J1810–197.

2. OBSERVATIONS, ANALYSIS, AND RESULTS

2.1. Radio Spectrum

We observed PSR J1550–5418 on four occasions with the Australia Telescope Compact Array (ATCA) interferometer,

TABLE 1
ATCA OBSERVATIONS OF PSR J1550–5418

Date	Flux calibrator	Frequency ν (GHz)	S_ν (mJy)
2007 Jun 26 ^a	0823–500	1.384	3.3 ± 0.3
		2.368	5.3 ± 0.3
2007 Jul 10	0823–500	1.384	4.4 ± 0.4
		2.368	5.4 ± 0.3
		4.800	6.4 ± 0.3
		8.640	5.5 ± 0.2
2007 Jul 24	1934–638	4.800	5.0 ± 0.2
		8.640	4.3 ± 0.2
		18.496	2.8 ± 0.2
		18.624	2.8 ± 0.2
2007 Aug 20	1921–293 ^b	42.944	5.6 ± 1.2
		44.992	5.6 ± 0.7

NOTE. — The array configuration was H168 for the last epoch, and 6C for all others. We used 1613–586 as the phase calibrator in all instances. In every case, at each frequency we sampled a bandwidth of 128 MHz in each of two orthogonal linear polarizations, and visibilities were accumulated into 32 pulsar phase bins.

^a Antennas CA01 and CA05 were off line.

^b Uranus was observed following our session to tie the flux scale to an absolute standard.

with the primary goal of measuring its radio spectrum. The observations were always done in pulsar-gated mode using the known ephemeris, and in each case we obtained pulse profiles with 32 phase bins in all Stokes parameters. The first observation, at simultaneous frequencies of 1.4 and 2.4 GHz, was already reported in Camilo et al. (2007b). Details of all observations are given in Table 1. Typically we first observed the flux calibrator and then interleaved ≈ 1 –2 minute observations of the pulsar (at higher radio frequencies we observed the phase calibrator more frequently). Two frequency bands were always observed simultaneously (in the middle two epochs we interleaved observations at 4.8 and 8.6 GHz with the other frequency pair; see Table 1). The integration times on the pulsar varied substantially, ranging between 2 and 6 hr for each

¹ Columbia Astrophysics Laboratory, Columbia University, New York, NY 10027.

² Australia Telescope National Facility, CSIRO, Parkes Observatory, Parkes, NSW 2870, Australia.

³ Australia Telescope National Facility, CSIRO, Epping, NSW 1710, Australia.

⁴ National Radio Astronomy Observatory, Charlottesville, VA 22903.

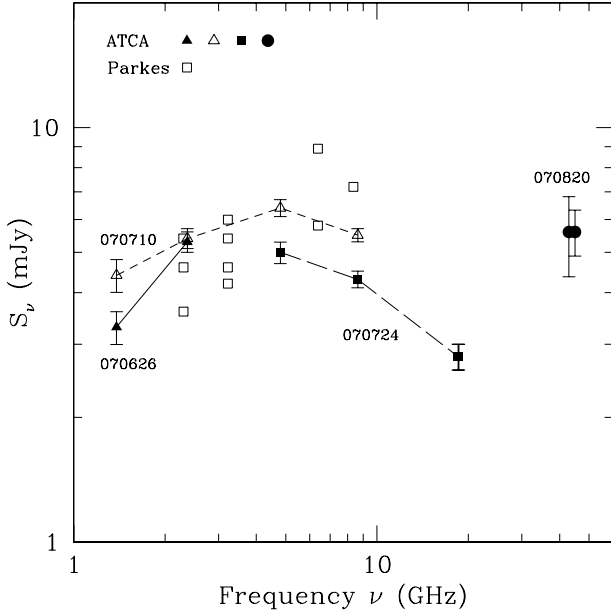


FIG. 1.— Flux densities of PSR J1550–5418 at 1.4–45 GHz. All points with error bars were derived from data obtained at the ATCA on four separate dates, labeled. Data collected at multiple frequencies on the same day are connected by lines. Open squares represent flux-calibrated measurements obtained at Parkes with a digital filterbank (see text) and have typical fractional uncertainties of about 25%.

frequency pair. With the array configurations used, we were in effect sensitive only to point sources.

We analyzed all data sets in a uniform manner using standard techniques with MIRIAD⁵. The 7 mm (30–50 GHz) system is new at the ATCA, and we took particular care to obtain the reported fluxes. The flux densities we used for the flux calibrator, 10.65 Jy at 43 GHz and 10.72 Jy at 45 GHz, were obtained immediately following our observations in a monitoring program using Uranus to tie 7 mm fluxes to an absolute scale. We also used the option “opcorr” in the MIRIAD task `atlod` in order to determine fluxes corrected for atmospheric opacity. All ATCA flux density measurements and uncertainties (Table 1 and Fig. 1) were obtained with the task `imfit`.

Using the Parkes radio telescope we observed PSR J1550–5418 with a digital filterbank (PDFB1 or PDFB2; Manchester 2006) at five different frequencies, on a total of 12 occasions. The main goal of these observations was to obtain calibrated polarimetric profiles (§ 2.2), but we also measured the flux densities. The Hydra A flux standard was observed at each epoch, and the data were analyzed with PSRCHIVE (Hotan et al. 2004). The resulting flux density measurements have an estimated fractional uncertainty of $\sim 25\%$, dominated by systematics in profile baselines, and are shown in Figure 1.

It is clear from Figure 1 that the flux density of PSR J1550–5418 varies with time. With an integrated column density of free electrons $DM = 830 \text{ cm}^{-3} \text{ pc}$, this variability cannot be ascribed to interstellar scintillation but rather is intrinsic (Camilo et al. 2007b). At each frequency for which multiple observations exist, the variability appears to be of order $\sim 30\%$ about the mean, but can reach $\sim 50\%$.

Most ordinary pulsars have steep radio power law spectra (Lorimer et al. 1995), with $\alpha < -1$ ($S_\nu \propto \nu^\alpha$). The spectrum of PSR J1550–5418 is very different. It is remarkably

flat over the range 1.4–45 GHz, but apparently cannot be described by one spectral index. Neglecting the data points at $\nu \approx 44$ GHz, the spectrum could be described as approximately log parabolic with a peak at ≈ 6 GHz. However, the precise description of the spectrum at $\nu > 9$ GHz requires greater reliability than is provided by the single-epoch measurements at ≈ 18 and 44 GHz, and further observations are required to clarify this.

2.2. Polarimetry

We have obtained polarimetric data from PSR J1550–5418 at Parkes on 12 occasions between 2007 July 5 and October 9. We used five different feed/receiver combinations: central beam of the 20 cm multibeam receiver (1.4 GHz), Galileo (2.3 GHz), 10/50 cm (3 GHz), central beam of the methanol multibeam receiver (6.4 GHz), and Mars (8.4 GHz). For the most recent 3 GHz observation (inset in Fig. 2) we recorded data with a 1 GHz bandwidth digital filterbank (PDFB2); at 8.4 GHz we used PDFB2 with 512 MHz of bandwidth. In all other instances we recorded 256 MHz of band with PDFB1. Typically ~ 10 pulse periods were folded in each subscan with 2048 bins across the pulse profile (1 ms resolution), and scans lasting up to ~ 1 hr were interspersed with ~ 1 minute observations of a pulsed calibrating signal in order to determine the relative gains and phases of the two feed probes in each receiver. At each epoch we also observed the Vela pulsar in order to provide a check on our polarimetric calibration, and Hydra A in order to obtain calibrated flux density measurements (see § 2.1). All data were analyzed with PSRCHIVE. Further details concerning the instrumentation and data analysis can be found in Camilo et al. (2007d).

Faraday rotation affects polarized radiation as it traverses the magnetized ISM. We determined the rotation measure of PSR J1550–5418 by measuring its position angle of linear polarization (P.A.) as a function of frequency within each 256 MHz band at 2.3, 3.2, and 6.4 GHz. The resulting $RM = -1860 \pm 20 \text{ rad m}^{-2}$ is the largest known for any pulsar. Together with the DM, it implies an average magnetic field strength along the line of sight weighted by electron density of $1.2 RM/DM = 2.7 \mu\text{G}$. Near this line of sight, $(l, b) = (327^\circ, 0^\circ)$, a number of compact radio sources have $RM \approx -1000 \text{ rad m}^{-2}$ (Gaensler et al. 2001), so that the large-scale Galactic field in this direction may be able to account for the extreme RM of PSR J1550–5418. Also near this direction, all pulsars at distance $\lesssim 5 \text{ kpc}$ have very small RM (Han et al. 2006), suggesting that PSR J1550–5418 is more distant, compatible with the DM-derived $d \approx 9 \text{ kpc}$.

In Figure 2 we show representative polarimetric profiles of PSR J1550–5418 at 1.4, 2.3, 3.2, 6.4, and 8.4 GHz (as shown by the insets at 3.1 and 6.4 GHz, sometimes the profiles vary). In each, the RM has been used to correct the frequency-integrated linear polarization and the observed P.A. to infinite frequency. It is evident from the figure that usually at $\nu \gtrsim 3$ GHz the emission is $> 90\%$ linearly polarized throughout the profile. At lower frequencies, however, the fraction of linear polarization is reduced: to about 80% at 2.3 GHz, and 25% at 1.4 GHz. At these frequencies the profile is scatter-broadened due to multipath propagation in the ISM (Camilo et al. 2007b), and these two facts are partly related (see § 2.2.1). The profiles also show substantial circular polarization, the level of which decreases with increasing frequency, from $\gtrsim 30\%$ at 1.4 GHz to $\lesssim 10\%$ at 8.4 GHz.

The ATCA observations (§ 2.1) extend these results to higher frequencies: at $\nu \approx 18$ and 44 GHz, the radiation from

⁵ See <http://www.atnf.csiro.au/computing/software/miriad/>.

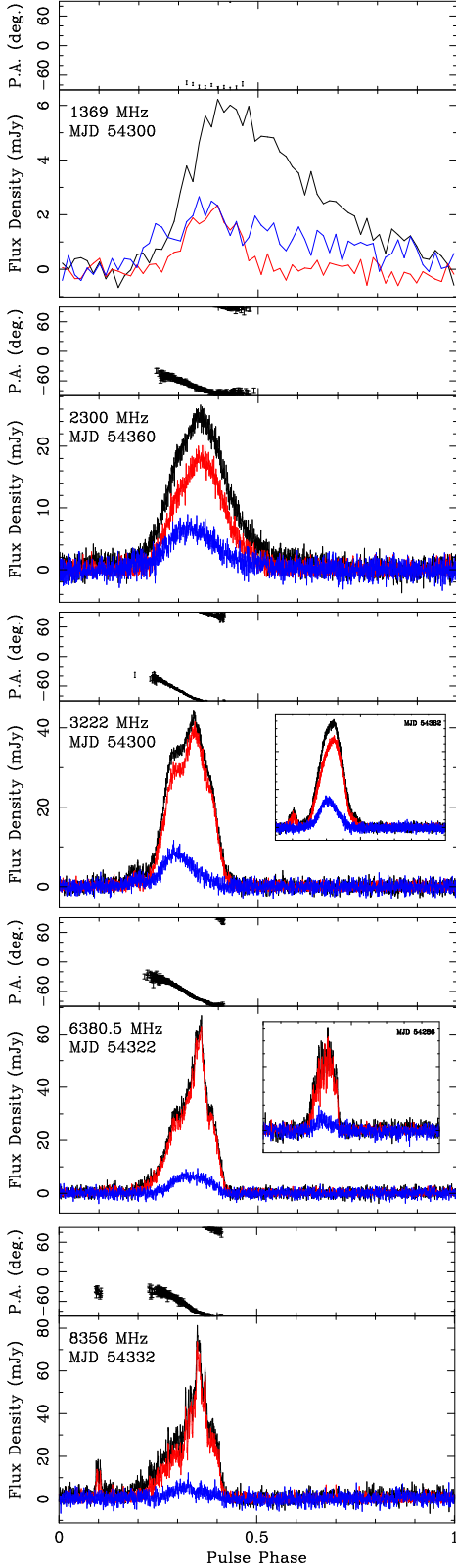


FIG. 2.— Representative polarimetric profiles of PSR J1550–5418 at frequencies of 1.4–8.4 GHz. The black, red, and blue lines represent, respectively, the total intensity and the amount of linear and circular polarization (Stokes parameters I , $L = (Q^2 + U^2)^{1/2}$, and V). The position angles ($\text{P.A.} = \frac{1}{2} \arctan(U/Q)$) are shown for bins where the L signal-to-noise ratio > 4 , and have been corrected for RM to their values at infinite frequency. The 1.4 GHz profiles are displayed with 64 phase bins; all others, with 2048 bins.

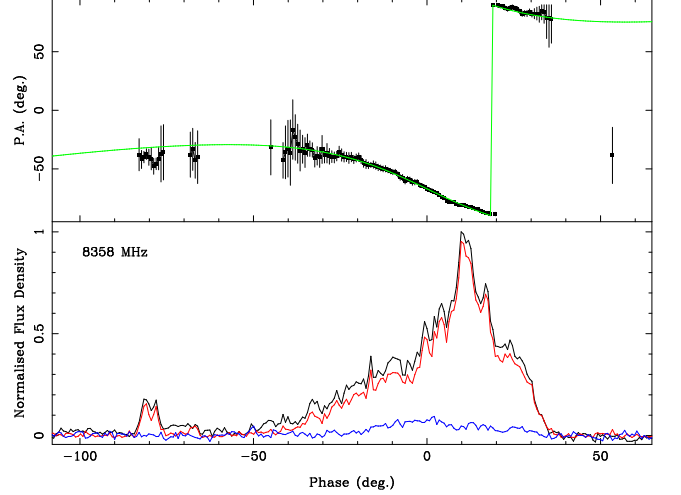


FIG. 3.— *Bottom*: Polarimetric profile of PSR J1550–5418 at 8.4 GHz with 170 degrees of pulse phase shown. The black trace shows the total intensity, with the red and blue showing linear and circular polarization respectively. *Top*: P.A. data (black points) and the RVM assuming $\alpha = 160^\circ$, $\beta = 14^\circ$. Here we are using the definitions of α and β given by Everett & Weisberg (2001). Here and in Fig. 4, the profiles are displayed with 512 bins per pulse period, and P.A. is plotted when the linear polarization signal-to-noise ratio > 2.5 .

PSR J1550–5418 remains approximately 100% linearly polarized throughout the profile (which, at ≈ 2 bins FWHM out of 32, appears to be somewhat narrower than at lower frequencies), and the level of circular polarization is $\lesssim 10\%$.

If certain assumptions are met (principally a dipole field geometry), the swing of P.A. as a function of pulse phase allows us to determine the geometry of the star, in particular the angle between its rotation and magnetic axes (α) and the impact parameter of the line of sight to the magnetic pole (β). Figure 3 shows the results of fitting the P.A. curve at 8.4 GHz to the rotating vector model (RVM; Radhakrishnan & Cooke 1969). Because of the wide longitude range over which this pulsar emits, constraints from the RVM fitting are good. We find that α must be greater than 140° (i.e., that the pulsar is almost aligned) and that $\alpha + \beta$ must be close to 180° , so that the line of sight remains largely within the beam at all times. This is confirmed by obtaining very similar results using data at 3 GHz that also show the presence of the initial leading component.

Figure 4 shows the alignment of the profiles at 3.2, 6.4 and 8.4 GHz. Zero phase has been assigned from the RVM fit at 3.2 and 8.4 GHz, with the 6.4 GHz profile aligned by eye. A number of features are readily apparent. The bulk of the emission covers some 80° of pulse phase, with the midpoint at the location of the steepest swing of P.A.. At 3.2 GHz there are at least three main pulse components visible: one near -20° , one near $+5^\circ$, and one near $+25^\circ$, with each of the three having roughly equal amplitude. At 6.4 and 8.4 GHz, the first component is substantially reduced in amplitude compared to the other two. Finally, at 8.4 GHz and occasionally at 3 GHz a precursor component is seen at phase -80° . The alignment of the position angles at all three frequencies is remarkable especially over such a large longitude range.

2.2.1. Depolarization

The pulses from PSR J1550–5418 are close to 100% linearly polarized at $\nu \geq 3$ GHz, with a modest component of circular polarization that decreases with increasing frequency. The linear polarization is evidently smaller at 2.3 GHz, and

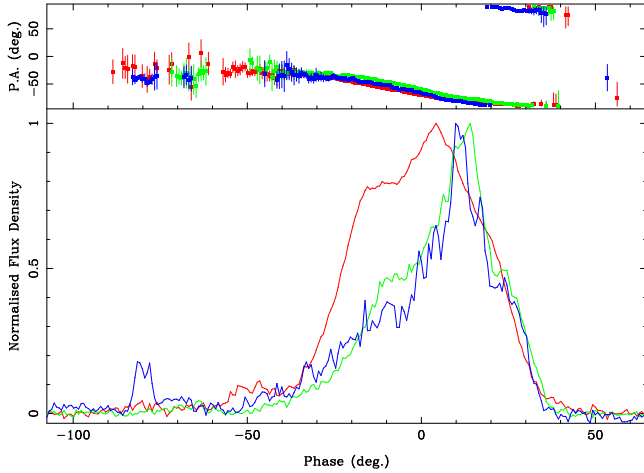


FIG. 4.— Total intensity profiles (*bottom*) and P.A.s (*top*) for PSR J1550–5418 at three frequencies (red corresponds to 3.2 GHz data, green to 6.4 GHz, and blue to 8.4 GHz). The P.A.s are corrected for an RM of -1860 rad m^{-2} and represent the (frequency independent) values at the pulsar. The point of zero phase is located at the steepest gradient of the P.A. swing.

strikingly more so at 1.4 GHz (Fig. 2). While this frequency dependence of polarization may be an intrinsic property of the pulsar, we must also consider the effects of interstellar scattering, which severely broadens the pulse at 1.4 GHz with a 1 s timescale (see top panel of Fig. 2; Camilo et al. 2007b). At 2.3 GHz, the pulse appears to be only slightly broadened in comparison with higher frequencies, which is consistent with the expected ν^{-4} dependence of the scattering timescale for scatterers of a single characteristic size: $\tau_{1.4} \approx 1 \text{ s}$ at 1.4 GHz corresponds to $\tau_{2.3} \approx 0.14 \text{ s}$ at 2.3 GHz.

Scattering is expected to reduce the linear polarization because the P.A. rotates through the different phases of the pulse, which are blended at the observer. This effect can be modeled at 2.3 GHz by assuming that the intrinsic pulse is similar to that observed at 3.2 GHz. Following Li & Han (2003) we convolve the individual Stokes parameters I, Q, U, V at 3.2 GHz with the function $g(t) = \exp(-t/\tau_{2.3})/\tau_{2.3}$ for $t > 0$, representing a thin scattering screen, varying $\tau_{2.3}$ to best fit the total intensity profile at 2.3 GHz. The result of this model is shown in Figure 5. A good representation of the 2.3 GHz I profile is obtained with $\tau_{2.3} = 0.145 \text{ s}$. The expected effects on the polarization are clearly seen in the model, namely, a reduction in the percentage of linear polarization, $(Q^2 + U^2)^{1/2}/I$, and a flattening of the P.A. curve on the trailing side of the pulse. But scattering does not fully account for the observed reduction in linear polarization at 2.3 GHz. The model predicts maximum linear polarization of 85% at the place where the observed is 79% (see top panel of Fig. 5). The data also show a flattening of the P.A. angle on the trailing side of the pulse, although it does not quite match the model on the leading side. We also applied a model of scattering from a medium extended between the source and observer (Williamson 1972; Li & Han 2003), which produces similar results and therefore is not shown here. At 1.4 GHz the difference between similar scattering models and the observed profiles is much greater. This is easy to understand: if the range of P.A.s emitted at 1.4 GHz is as limited as those observed at $\nu \geq 3 \text{ GHz}$, no amount of scattering can mix those P.A.s to yield the very low level of linear polarization observed at 1.4 GHz (top panel of Fig. 2).

Another interstellar effect that may reduce the linear po-

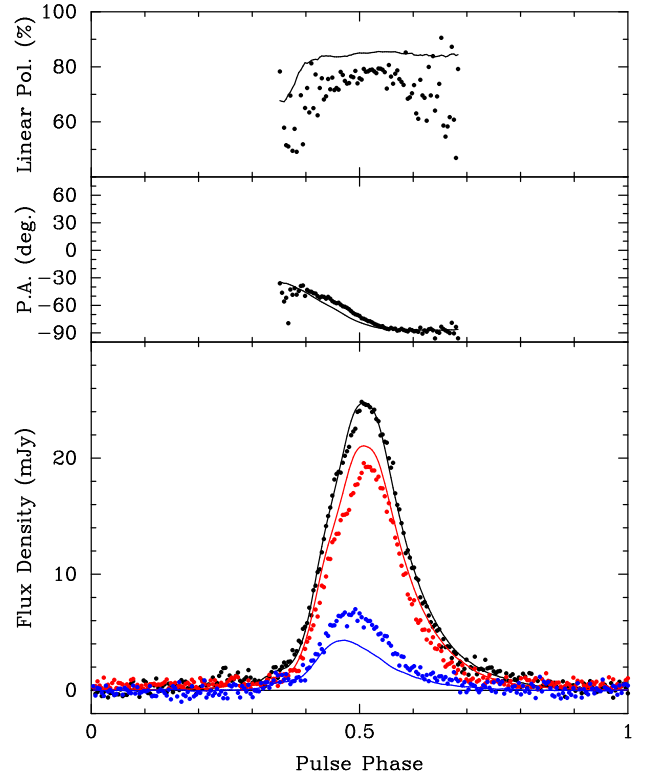


FIG. 5.— Observed 2.3 GHz profiles of PSR J1550–5418 (*dots*) and a model that consists of the 3.2 GHz Stokes parameters convolved with an exponential of $\tau_{2.3} = 0.145 \text{ s}$ (*solid lines*). The parameter $\tau_{2.3}$ was adjusted by eye to give a good fit to total intensity. Colors in the bottom panel are as in Fig. 2, and the relevant 3.2 and 2.3 GHz profiles are also shown in that figure. P.A. is plotted here between -100° and $+80^\circ$ in order for the data not to wrap around as it does in Fig. 2.

larization, without affecting the circular component, is deviations in RM over the different paths taken by the scattered rays. Non-uniformity of either the electron density or the magnetic field on transverse length scales a corresponding to the scattering timescale, $a \approx (cd\tau)^{1/2} = 1-3 \times 10^{16} \text{ cm}$, if large enough to change RM by $\sim 60 \text{ rad m}^{-2}$, or 3% of its measured value, would severely reduce linear polarization at 1.4–2.3 GHz by mixing the P.A.s. However, we do not explicitly model this ad hoc scenario here.

In summary, a scattering model accounts for only part of the observed reduction in linear polarization at low frequencies, and it has little effect on circular polarization. There is also an intrinsic effect in which circular polarization decreases with increasing frequency while linear polarization increases. Among ordinary pulsars, circular polarization increases with increasing frequency for some, but in others it decreases (You & Han 2006).

2.3. Timing

Since the discovery of pulsations from 1E 1547.0–5408 on 2007 June 8, we have timed the pulsar at Parkes on a regular basis. As of November 22, we have obtained times-of-arrival (TOAs) on 36 separate days. These have been derived from data collected with the analog filterbank used to discover pulsations, at all frequencies mentioned in § 2.2 according to receiver availability. Although the pulse profiles are different at separate frequencies (and sometimes vary even at one frequency; see Fig. 2), this does not affect greatly the overall timing precision, which is dominated by rotational instabili-

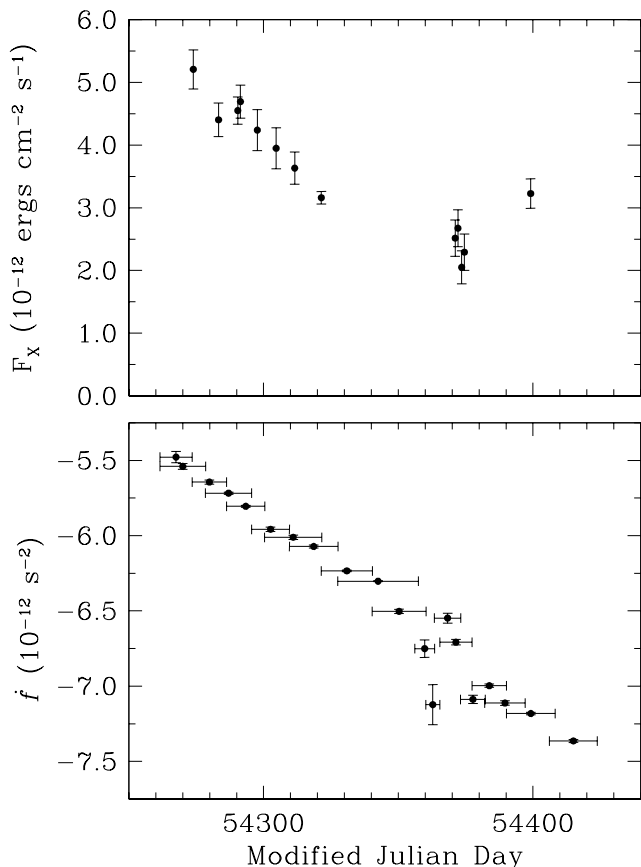


FIG. 6.— *Bottom*: Evolution of spin frequency derivative for PSR J1550–5418. All the data were obtained at Parkes, and each point is from a TEMPO fit to f and \dot{f} . After decreasing at a constant rate for 3 months, between MJD 54360 and 54365 \dot{f} decreased much more rapidly, and after fluctuating over the following 2 weeks, it has continued its trend. *Top*: Absorbed, 1–8 keV X-ray flux of 1E 1547.0–5408 (from Halpern et al. 2008).

ties in the neutron star.

We have tracked the rotational evolution of PSR J1550–5418 using TEMPO⁶ to fit the TOAs to models that include rotational phase, spin frequency $f = 1/P$, and \dot{f} (the celestial coordinates were held fixed at the values obtained from ATCA data; see Camilo et al. 2007b). When the data span exceeds approximately 1 month, these models no longer describe well the behavior of the star. As is common for magnetars that display substantial “timing noise,” the addition of higher frequency derivatives to the model can improve the timing fit, although without predictive value. Instead here, in Figure 6, we present the results of piece-wise fits to f and \dot{f} . In order to better sample the variation of \dot{f} , the time intervals used to obtain these fits were made as short as possible consistent with a relatively small uncertainty for \dot{f} .

For the first 3 months of our monitoring, \dot{f} decreased at a constant rate ($\dot{f} = -1.21 \times 10^{-19} \text{ s}^{-3}$), for a total decrease of about 20% compared to the initial value. Then, sometime within MJDs 54360–54365, \dot{f} quickly decreased further, and within the subsequent 2 weeks fluctuated before continuing its decreasing trend at the same rate as before (see bottom panel of Fig. 6). There is no indication that any permanent period step resulted from the interval of fluctuating \dot{f} . As of late

2007 November, the characteristic age of PSR J1550–5418 is $P/2\dot{P} = 1 \text{ kyr}$.

3. DISCUSSION

In the 6 months since the discovery of pulsations from PSR J1550–5418, its period derivative and torque have increased by about 40%. In magnitude, this level of “timing noise” is not unprecedented for magnetars. Quantifying timing noise as the magnitude of its cumulative contribution to the cubic term of a Taylor series expansion of rotational phase over a time interval t , i.e., $\dot{f}t^3/6$ (Arzoumanian et al. 1994), this amounts to about 60 cycles over 6 months, compared to 20 cycles over 9 months for the 5.5 s AXP XTE J1810–197 (Camilo et al. 2007a). However, the torque of XTE J1810–197 was decreasing, at a time when the neutron star was returning to quiescence years after a large outburst. As the torque decreased, so did the radio flux, which could indicate a decrease of particle flux in the magnetosphere that might itself be partly responsible for the decreased torque (see in this regard Kramer et al. 2006).

In PSR J1550–5418, the torque has been increasing, at a time when the X-ray flux has been generally decreasing (see Fig. 6). It appears that after the \dot{f} fluctuated in late 2007 September, the X-ray flux stabilized or even increased, but poor sampling of the light curve makes it hard to establish with confidence the correlative rotational–radiative behavior.

In any case, it remains unclear why torque should continue to increase while X-ray luminosity decreases. A logical explanation for the large excursions in spin-down rate of magnetars involves an extra torque (in addition to the magnetic dipole spin-down) derived from a particle wind that both “combs out” the magnetic field and carries additional angular momentum (Harding et al. 1999; Thompson et al. 2000). The luminosity of such winds is considered to be derived from either ongoing seismic activity, or static magnetospheric currents (Thompson et al. 2002), neither of which should correlate inversely with X-ray luminosity. (The radio luminosity, which is energetically inconsequential but may point to a substantial particle wind, so far shows no secular trend.) Even more dramatic deviations of torque evolution from X-ray luminosity were observed from the AXP 1E 1048.1–5937 (Gavril & Kaspi 2004): its X-ray flux increased by a factor of 4 over a period of 1 month, then decreased over 6 months to half its peak value, and stayed relatively constant for 1 year thereafter; in the meantime, the torque increased by a factor of 10 during the decay of the X-ray flux, and subsequently varied by factors of up to 3 in both directions during the period of stable X-ray flux. We have been observing 1E 1547.0–5408 since 2007 June, at least 2 months after its radio flux increased and up to 10 months after its X-ray flux increased by a factor of ≥ 16 (Halpern et al. 2008), and it remains to be seen how its long-term behavior compares to that of 1E 1048.1–5937.

Flux density variations such as observed in PSR J1550–5418, by up to $\sim 50\%$ on timescales of a few days (see Fig. 1), which cannot be accounted for by diffractive or refractive scintillation, are intrinsic and are not observed in ordinary pulsars. Also, the variability observed in its pulse profiles, two examples of which are shown in Figure 2, is unlike that of ordinary pulsars. Such changes are however observed in the other known radio magnetar, XTE J1810–197, where they are even more striking (Camilo et al. 2007a). Although the cause of these variations is not known, they may be related to changes in magnetospheric plasma densities and/or currents

⁶ See <http://www.atnf.csiro.au/research/pulsar/tempo/>.

that might also affect the torque on the neutron star.

The radio spectrum of PSR J1550–5418 (Fig. 1) is remarkable (we neglect here the apparent dip at $\nu \approx 18$ GHz which, if real, would make it even more remarkable; due to observed variability at lower frequencies and only one observation at each of ≈ 18 and 44 GHz, we consider this dip as tentative). Although its flux density at 1.4 GHz is not particularly large (10% of known pulsars have a larger value), at 45 GHz no pulsar is presently brighter (see, e.g., Kramer et al. 1997). In this regard, PSR J1550–5418 is similar to XTE J1810–197, which has an approximately flat (and variable) spectrum between 0.3 and 144 GHz ($-0.5 \lesssim \alpha \lesssim 0$; Camilo et al. 2007c). The reason for this is not known but it is also not understood, after 40 years, why ordinary pulsars have steep spectra, with $\langle \alpha \rangle = -1.6$. The differences observed between the radio spectra of ordinary pulsars and magnetars could be important clues to both of their emission processes. Whether they are caused, e.g., by different particle population and acceleration mechanisms, or by magnetospheric propagation effects, remains to be investigated.

The flat spectrum of PSR J1550–5418 has allowed us to measure its polarimetric properties up to 45 GHz, a record among pulsars. The slow sweep of P.A. and its absolute value are identical at all frequencies observed (see Fig. 4), as expected in the RVM. Also, the overall pulse profile is wide and highly linearly polarized with relatively little evolution with frequency (with the possible exception of low frequencies). These characteristics are similar to those of the radio AXP XTE J1810–197 (Camilo et al. 2007d), and to those of young ordinary pulsars (Johnston & Weisberg 2006). Therefore, while unexpected a priori, it appears that ideas developed to understand the geometry of emission from ordinary pulsars along open dipolar magnetic field lines also apply to both known radio magnetars.

For PSR J1550–5418, the results of the RVM fits (§ 2.2) imply that the rotation and magnetic axes are nearly aligned. Therefore, even though the polar cap radius, $\propto P^{-1/2}$, is small, the observed profile is wide because the line of sight remains largely within the emission beam. The radio beaming fraction for such a magnetar, however, is expected to be small. Conversely, for XTE J1810–197 we determined that the most likely geometry is one with a substantial misalignment between the rotation and magnetic axes, and a correspondingly large beaming fraction (and also emission height; Camilo et al. 2007d). For XTE J1810–197, the RVM fits also allow for a formally good solution with aligned axes, but we prefer the misaligned geometry because it better explains the large observed modulation of thermal X-rays (this is shown in great detail in the modeling of Perna & Gotthelf 2008). For PSR J1550–5418, on the other hand, the very small observed X-ray modulation (Halpern et al. 2008) is more compatible with the nearly aligned geometry preferred from our RVM

fits.

The aligned geometry does not constrain emission height. However, Johnston & Weisberg (2006) showed that emission from a cone high in the magnetosphere could explain many observed properties of young pulsars, and the properties of PSR J1550–5418 are consistent with this picture. Also unlike in XTE J1810–197 (Camilo et al. 2007d), it is not clear whether there is any evidence in PSR J1550–5418 that higher radio frequencies are emitted closer to the star than lower frequencies, since the width of pulse components does not clearly decrease with increasing frequency (see Fig. 4). A final difference between the polarimetric characteristics of the two known radio AXPs is that in XTE J1810–197 the level of circular polarization is very small ($< 10\%$) and does not change with frequency, while in PSR J1550–5418 the circular polarization is larger and increases with decreasing frequency, as the linear polarization decreases.

Based on our study of the two known radio magnetars, we can identify significant common properties: both pulsars are very highly linearly polarized; both have very flat spectra over a wide range of frequencies; both have variable pulse profiles and radio flux densities. The first of these properties is also common with many ordinary young pulsars, while the latter two are exceptional. The cause of these traits is not known, and their understanding would greatly increase our knowledge of the magnetospheres of highly magnetized neutron stars. It is also not known why these are the only two magnetars so far to have been detected at radio wavelengths. XTE J1810–197 is clearly a transient AXP, in the sense that in quiescence its surface temperature is as low as that of some ordinary young neutron stars (Gotthelf et al. 2004). However, this is not obviously the case with 1E 1547.0–5408 (see Halpern et al. 2008), and it may bear more of a resemblance to “persistent” AXPs. Its radio emission appears to make it unusual among AXPs, but it has a small beaming fraction and is only transiently detectable (Camilo et al. 2007b). Therefore, without any existing theoretical basis for excluding radio emission from magnetars, it seems reasonable to suppose that any magnetar could in fact occasionally emit radio waves.

We thank Michael Dahlem for his generous help, particularly with calibrating ATCA 7 mm data, John Sarkissian for observing assistance, and the dedicated staff at Parkes. Willem van Straten kindly helped with the PSRCHIVE software. We are grateful to Phil Edwards and Dave McConnell for quickly approving and scheduling the observations at the ATCA. The Parkes Observatory and the ATCA are part of the Australia Telescope, which is funded by the Commonwealth of Australia for operation as a National Facility managed by CSIRO. This work was supported in part by the NSF through grant AST-05-07376 to F.C.

REFERENCES

- Arzoumanian, Z., Nice, D. J., Taylor, J. H., & Thorsett, S. E. 1994, *ApJ*, 422, 671
- Camilo, F., Cognard, I., Ransom, S. M., Halpern, J. P., Reynolds, J., Zimmerman, N., Gotthelf, E. V., Helfand, D. J., Demorest, P., Theureau, G., & Backer, D. C. 2007a, *ApJ*, 663, 497
- Camilo, F., Ransom, S. M., Halpern, J. P., & Reynolds, J. 2007b, *ApJ*, 666, L93
- Camilo, F., Ransom, S. M., Halpern, J. P., Reynolds, J., Helfand, D. J., Zimmerman, N., & Sarkissian, J. 2006, *Nature*, 442, 892
- Camilo, F., et al. 2007c, *ApJ*, 669, 561
- Camilo, F., Reynolds, J., Johnston, S., Halpern, J. P., Ransom, S. M., & van Straten, W. 2007d, *ApJ*, 659, L37
- Duncan, R. C., & Thompson, C. 1992, *ApJ*, 392, L9
- Everett, J. E., & Weisberg, J. M. 2001, *ApJ*, 553, 341
- Gaensler, B. M., Dickey, J. M., McClure-Griffiths, N. M., Green, A. J., Wieringa, M. H., & Haynes, R. F. 2001, *ApJ*, 549, 959
- Gavril, F. P., & Kaspi, V. M. 2004, *ApJ*, 609, L67
- Gelfand, J. D., & Gaensler, B. M. 2007, *ApJ*, 667, 1111
- Gotthelf, E. V., Halpern, J. P., Buxton, M., & Bailyn, C. 2004, *ApJ*, 605, 368
- Halpern, J. P., Gotthelf, E. V., Becker, R. H., Helfand, D. J., & White, R. L. 2005, *ApJ*, 632, L29

- Halpern, J. P., Gotthelf, E. V., Reynolds, J., Ransom, S. M., & Camilo, F. 2008, *ApJ*, in press (arXiv/0711.3780)
- Han, J. L., Manchester, R. N., Lyne, A. G., Qiao, G. J., & van Straten, W. 2006, *ApJ*, 642, 868
- Harding, A. K., Contopoulos, I., & Kazanas, D. 1999, *ApJ*, 525, L125
- Hotan, A. W., van Straten, W., & Manchester, R. N. 2004, *Proc. Astr. Soc. Aust.*, 21, 302
- Ibrahim, A. I., et al. 2004, *ApJ*, 609, L21
- Johnston, S., & Weisberg, J. M. 2006, *MNRAS*, 368, 1856
- Kramer, M., Jessner, A., Doroshenko, O., & Wielebinski, R. 1997, *ApJ*, 489, 364
- Kramer, M., Lyne, A. G., O’Brien, J. T., Jordan, C. A., & Lorimer, D. R. 2006, *Science*, 312, 549
- Kramer, M., Stappers, B. W., Jessner, A., Lyne, A. G., & Jordan, C. A. 2007, *MNRAS*, 377, 107
- Li, X. H., & Han, J. L. 2003, *A&A*, 410, 253
- Lorimer, D. R., Yates, J. A., Lyne, A. G., & Gould, D. M. 1995, *MNRAS*, 273, 411
- Manchester, R. N. 2006, *Chin. J. Astron. Astrophys.*, 6, 139
- Perna, R., & Gotthelf, E. V. 2008, *ApJ*, submitted
- Radhakrishnan, V., & Cooke, D. J. 1969, *Astrophys. Lett.*, 3, 225
- Thompson, C., & Duncan, R. C. 1995, *MNRAS*, 275, 255
- . 1996, *ApJ*, 473, 322
- Thompson, C., Duncan, R. C., Woods, P. M., Kouveliotou, C., Finger, M. H., & van Paradijs, J. 2000, *ApJ*, 543, 340
- Thompson, C., Lyutikov, M., & Kulkarni, S. R. 2002, *ApJ*, 574, 332
- Williamson, I. P. 1972, *MNRAS*, 157, 55
- Woods, P. M., & Thompson, C. 2006, in *Compact Stellar X-ray Sources*, ed. W. H. G. Lewin & M. van der Klis (Cambridge: Cambridge Univ. Press), 547–586
- You, X.-P., & Han, J.-l. 2006, *Chin. J. Astron. Astrophys.*, 6, 237